Efficient catalytic ozonation by ruthenium nanoparticles supported on SiO2 or TiO2: Towards the use of a non-woven fiber paper as original support

Pierre-Francois Biard, Baraa Werghi, Isabelle Soutrel, Romain Orhand, Annabelle Couvert, Audrey Denicourt-Nowicki, Alain Roucoux

Efficient catalytic ozonation by ruthenium nanoparticles supported on SiO_2 or TiO_2: Towards the use of a non-woven fiber paper as original support

Pierre-François BIARD[a,b*], Baraa WERGHI[c] , Isabelle SOUTREL[a,b], Romain ORHAND[a,b], Annabelle COUVERT[a,b], Audrey DENICOURT-NOWICKI[a,b], Alain ROUCOUX[a,b]

[a] École Nationale Supérieure de Chimie de Rennes, CNRS, UMR 6226, 11 Allée de Beaulieu, CS 50837, 35708 Rennes Cedex 7, France

[b] Université européenne de Bretagne, 5 boulevard Laënnec, 35000 Rennes, France

[c] KAUST Catalysis Center, 4700 KAUST, Thuwal 23955-6900, Saudi Arabia

Abstract

This work focuses on the use of Ru(0) nanoparticles as heterogeneous catalyst for ozone decomposition and radical production. In a first set of experiments, the nanoparticles have been deposited on two inorganic supports (TiO_2 or SiO_2) by a wet impregnation approach. This study confirmed the high potential of Ru nanoparticles as active species for ozone decomposition at pH 3, since the ozone half-life time decreases by a factor 20-25, compared to the reference experiment carried out without any catalyst. The enhancement of the ozone decomposition kinetics provided an improved radical production and a higher transient radical concentration in a shorten ozone exposure. Consequently, lower oxidant dosage and contact time would be necessary. Thus, very significant atrazine consumption kinetics enhancements were measured. In a second set of experiments, a non-woven fiber paper composed of a TiO_2/SiO_2/zeolite mixture has been evaluated as an original support for ruthenium nanoparticles. Even if lower ozone decomposition kinetics was observed compared to TiO_2 or SiO_2, this support would be a promising alternative to inorganic

* Corresponding author : pierre-francois.biard@ensc-rennes.fr, +33 2 23 23 81 57

powders to avoid the catalyst recovery step and to design reactors such as tubular reactors. A new numerical procedure is presented for the evaluation of the transient HO° concentration and of the R_{ct}.

Key words

Ozone; catalyst; catalytic ozonation; ruthenium nanoparticles; micropollution

Highlights

- The potential of supported ruthenium nanoparticles in catalytic ozonation was investigated
- SiO_2, TiO_2 and a non-woven fiber paper were used as support for nanoparticles
- Ru/SiO_2 and Ru/TiO_2 catalysts are more effective for O_3 decomposition than SiO_2 and TiO_2
- Ru/SiO_2 and Ru/TiO_2 catalysts are more effective for radical generation than SiO_2 and TiO_2
- The potential of a non-woven fiber paper as Ru nanoparticles support is demonstrated

1. Introduction

Micropollutants (pesticides, dyes, pharmaceutical products, etc.) removal is one of the main challenges faced in water treatment. Besides biological and physical methods, chemical approaches based on oxidation and mineralization in harmless byproducts (mainly H_2O and CO_2) can be used for micropollutant remediation [1, 2].

With a high oxidant potential, ozone remains a pertinent candidate among other oxidants (chlorine, hydrogen peroxide, etc.). However, owing to its selective character, its application for this purpose has been limited. Advanced Oxidation Processes (AOPs) are water and air treatment processes based on the generation of hydroxyl radicals HO°, which are powerful and non selective oxidants, using mild conditions (ambient temperature and atmospheric pressure) [3, 4]. Most of the time, radical chain mechanisms are involved in AOPs based on the decomposition of an oxidant (O_3, H_2O_2), initiated by a physical (UV, ultrasound, etc.) or a chemical factor. Thus, the ozone decomposition can be initiated by the hydroxide anion (HO^-), the hydroperoxide anion HO_2^-, UV radiation, homogeneous catalysts (Mn(II), Fe(II), etc.) and heterogeneous catalysts [5, 6].

Since the 1990s, numerous research studies have been focusing on the combined application of ozone with solid catalysts (activated carbon, zeolites, metal oxides, etc.), since their active surfaces can increase the ozone decomposition kinetics [5]. Usually, the activity of these species is maintained over time which justifies the term “catalyst”. The mechanism is particularly difficult to investigate and involves both physical (adsorption, internal and external diffusions of the ozone, the pollutant, the by-products, etc.) and chemical steps (reactions at the solid-liquid interface). As mentioned by Nawrocki and Kasprzyk-Hordern, all active sites (Lewis centers and non-dissociated hydroxyl groups of metal oxides, basic centers of activated carbon, etc.) were considered as potential catalytic sites for ozone decomposition [7, 8]. As recently mentioned by Zhao et al. (2015), the simple preparation of an efficient and stable catalyst for heterogeneous catalytic ozonation with high surface area is still highly challenging [9].

More recently, metal and metal oxides nanoparticles have proved to be promising catalysts for ozone decomposition, owing to their high surface specific area and a high number of surface-exposed atoms [10-16]. These nanoparticles are usually deposited on a support to facilitate their recovery and finally to increase their durability. They have demonstrated a good potential for ozone decomposition. However, a comparison of these various nanocatalysts remains tricky, since different operating conditions are usually implemented (pH, nature of the targeted pollutant, ozone, pollutant and catalyst concentrations, flow conditions, mixing intensity, temperature, etc.). Moreover, even if the potential for the ozone decomposition is demonstrated, the potential for the HO° radical generation is often not evaluated. Most of the time, these nanoparticles are heterogeneized on powders or pellets such as metallic oxides (silica, titanium dioxide, etc.), inorganic supports (zeolite, clays, etc.) and carbon (activated, graphite, etc.) [5, 7, 8]. Powders are usually preferred because external diffusion limitations are rare [5]. Nevertheless, depending on the size of the support, the catalyst recovery from the treated water is complicated even if new magnetic catalysts are now developed to easily recover them using magnets [17, 18]. Few studies focused on fixed supports such as monoliths, which are appealing because of an easy implementation at industrial scale [19]. Ceramic honeycombs have been particularly investigated by a Chinese team [20-22]. Indeed, monolithic catalysts offers several benefits such as a reduced pressure drop, an improved mass-transfer and an easier catalyst separation as compared to reactor filled with pellets [23]. Moreover, their implementation as fixed bed is particularly appealing. Nevertheless, the coating of the monolith with the active catalyst is often complex.

This study focuses on the potential of metal nanoparticles deposited on various inorganic supports for ozone decomposition and HO° production. After a preliminary screening, ruthenium has been selected among other metals (Co, Pd, Pt, Rh), owing to its better reactivity in a low charge (0.1% wt) associated to a rather low cost (≈ 30 Euros/g). This good efficiency of ruthenium species (2% wt) coated on cerium dioxide by impregnation has already been reported in the literature [24]. Here, the

deposition was performed through a mild and easy procedure based on a wet impregnation of well-controlled nanometric size metal particles, as previously described [25, 26].

Two powder inorganic supports, TiO_2 and SiO_2, have been chosen as pertinent supports for metal nanospecies and the obtained nanocomposites were evaluated for catalytic ozonation. The catalytic experiments were conducted in batch mode using a free headspace reactor to avoid ozone desorption. An acidic pH (≈ 2.9) has been selected to prevent ozone decomposition initiation by the hydroxide anion. No buffer was added since they can be chemisorbed competitively with the ozone on the active sites (especially phosphate buffers) and influence the ozone decomposition kinetics [7]. Atrazine, a well-known micropollutant substrate was used as a HO° radical tracer and was added at a very low concentration (≈ 250 ppb) to limit its influence (and those of its by-products) on the ozone decomposition and active species generation. This operating condition enables to compare the catalysts on a rigorous basis taking into account only the mechanism of the ozone decomposition on the catalyst surface. Atrazine has been widely used as herbicide [27]. Its concentration in surface and ground waters has been frequently detected above the maximum permissible level in Europe [28]. Atrazine is poorly biodegradable and recalcitrant to ozone oxidation. However, its oxidation by hydroxyl radicals is effective and leads to cyanuric acid as final product with several intermediates [28].

Finally, the potential of a fixed support, a non-woven fiber paper, has also been evaluated as an original and industrially promising support and compared to the previous powder supports. To our knowledge, the use of a flexible fixed support in catalytic ozonation is a novel and unprecedented approach, which could offer a pertinent technique for micropollutant removal and an easy implementation. Indeed, the design of tubular reactors (tangential flow) or reactors composed of successive layers of papers (crossing flow) could be imagined.

2. Material and methods

2.1 Catalyst preparation

Three different supports were used for the heterogeneization of Ru(0) nanoparticles (NPs)* : anatase TiO_2, keatite SiO_2, which are powder supports, and a 250 µm thick porous paper. This media, provided by the Ahlstrom Company, under the reference Ahlstrom _1048, is composed of cellulose fibers coated with a mixture of TiO_2 (13.3 g m^{-2}), SiO_2 (16.7 g m^{-2}) and zeolite (3.4 g m^{-2}).

The Ru(0) nanospecies were deposited on these various supports through a wet impregnation methodology, already reported in the literature [25, 26, 29]. First, 100 mL of an aqueous suspension of ruthenium NPs was prepared by reducing ruthenium chloride precursor (3.8 x 10^{-4} mol $RuCl_3$. $3H_2O$) in the presence of sodium borohydride (2.5 eq.) as reducing agent, and N,N-dimethyl-N-cetyl-N-(2-hydroxyethyl) ammonium chloride (2 eq. HEA16Cl) as surfactant to protect particles in solution thus avoiding their aggregation, according to an already described approach [30-32]. In a second step, the irreversible adsorption of the ruthenium NPs on the TiO_2 or SiO_2 supports was achieved by a wet impregnation of the inorganic support with the pre-stabilized aqueous ruthenium suspension. After filtration and several water washings, the powder was dried for one day at 60°C. The final metal loading was 0.1 % wt., as determined by elementary analysis. Onto the non-woven fiber paper as support, the adsorption of the ruthenium particles on the material was achieved by percolation of a known volume of the pre-stabilized aqueous ruthenium suspension. The decolorization of the solution demonstrated the adsorption of the nanospecies on the paper. The paper was dried for one day at the ambient air or at 60°C to compare both methods.

* NPs : nanoparticles

2.2 Batch experiments

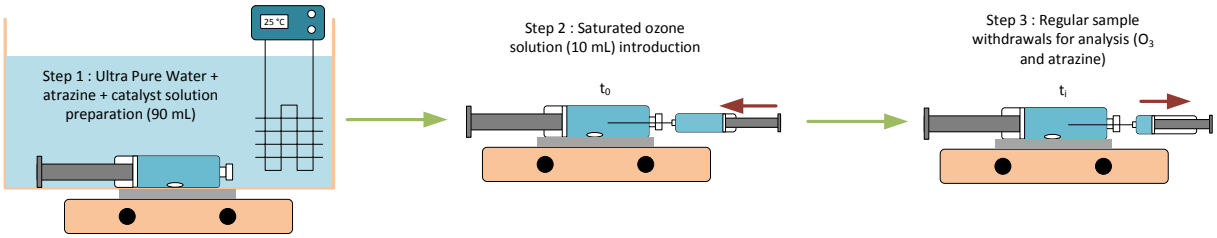

Figure 1. Experimental procedure description

The experiments were conducted batch-wise in a 100 mL glass gas-tight syringe (Hamilton) containing a stirring bar and equipped with a septum for solutions injections and sampling. The gas-tight syringe is convenient for ozone experiments since its volume can be adjusted owing to the plug and since the absence of gaseous headspace allows avoiding ozone stripping. This reactor was filled with 90 mL of a solution containing about 300 µg L^{-1} of atrazine (used as a radical probe [33]) and 250 to 1000 mg L^{-1} of catalyst (Fig. 1). This solution was prepared with ultrapure ozonated-deozonated water (whose pH naturally dropped to approximately 3). The reactor was well stirred and immersed in a thermostatic bath regulated at 25 °C. The pH of the solution was measured at 2.9 ± 0.1. In parallel, a saturated ozone solution at ≈ 20 ppm was prepared. 10 mL of this solution were injected at t=0 in the syringe and the time was recorded. Then, samples were withdrawn regularly and immediately injected in a known volume of a Indigo Carmine solution to quench the ozone residual (*i.e* stop the radical chain reaction) and to allow further ozone quantification. A volume of this mixture was kept for atrazine quantification.

2.3 Ozone generation

The ozone solution was prepared by gaseous ozone dissolution during at least 2 hours at 100 NL min^{-1} in a 2 L glass gas-liquid contactor (bubble column). Gaseous ozone was produced at approximately 100 g Nm^{-3} with a Trailigaz ozone generator fed with pure oxygen. Dissolved ozone at saturation concentrations used was analyzed before each experimentation with 3 withdrawals using

a gas-tight glass syringe (SGE). Values were obtained around 20 mg L^{-1}. Residual gaseous ozone was removed by an ozone destructor placed at the reactor outlet.

2.4 Atrazine analysis

Atrazine concentration was quantified by ULPC/MS/MS, using an Acquity UPLC (Waters corporation, USA) and a Quattro Premier triple quadrupole mass spectrometer equipped with an electrospray ionization source (ESI). A BEH C18 column (100 mm × 2.1 mm ID with 1.7 μm particle size) was used. The mobile phase (flow-rate of 400 μL min^{-1}) was composed of acetonitrile (55%) and ultra pure water (45%), both previously acidified with formic acid (0.1%). The oven temperature was 45 °C. The parameters of the spectrometer were a cone voltage = 35 V, a collision energy = 15 eV, an electrospray source block temperature = 120°C, a desolvatation temperature = 350°C, a capillary voltage = 3 kV, an argon collision gas pressure = $3.33x10^{-3}$ mbar, a cone gas (Nitrogen) flow rate = 75 L h^{-1} and a desolvatation gas (Argon) flow rate = 750 L h^{-1}. Mass Lynx software was used for instrumental control, data acquisition and quantification. Two transitions were selected for atrazine (216.08 $\rightarrow$ 173.8, the most abundant transition for quantification; 216.08 $\rightarrow$ 95.6 for confirmation).

2.5 Porosity – Nitrogen adsorption

Nitrogen physisorption isotherms were measured at 77 K using a volumetric gas sorption analyzer to determine the BET surface area of the catalysts (Autosorb-1-MP®, Quantachrome Instruments). Samples were previously outgassed at 250 °C for 48 h. Specific surface area was calculated by using the multipoint BET method. The total pore volume was calculated from the amount of gas adsorbed at a relative pressure of 1. The Non Linear Density Functional Theory (NLDFT) was used to analyze the pore size distribution of SiO_2 and Ru/SiO_2 considering cylindrical pores and a silica structure [34]. The calculation method was provided from Quantachrome Instruments.

3. Results and discussion

3.1 Catalysts' characterization

The supported nanocatalysts were easily obtained from wet impregnation of the inorganic support (SiO_2 or TiO_2) with aqueous suspensions of ruthenium nanoparticles. TEM analyses (Supporting Information) have showed that the well-dispersed preformed Ru particles possess sizes around 2.25 nm and from previous works, we could presume that similar sizes were obtained after heterogeneization on the inorganic support [25]. BET surface area has been measured by nitrogen physisorption. Impregnated and non-impregnated TiO_2 isotherms are not significantly different. The structure is poorly porous with a surface area of about 50 $m^2\ g^{-1}$. This porosity is mainly composed of mesopores. SiO_2 and SiO_2@Ru(0) NPs surface areas are significantly higher (around 450 $m^2\ g^{-1}$) and present both micropores and mesopores between 2 and 8 nm.

Even if the surface area of impregnated and non-impregnated SiO_2 is not significantly different, application of the DFT indicates that the mesopore size distribution changes with the impregnation (Fig. 2). Indeed, Ru(0) NPs are adsorbed on mesopores with a diameter around 4 nm and confirms the controlled size of the NPs. The micropores volume is not impacted by the impregnation.

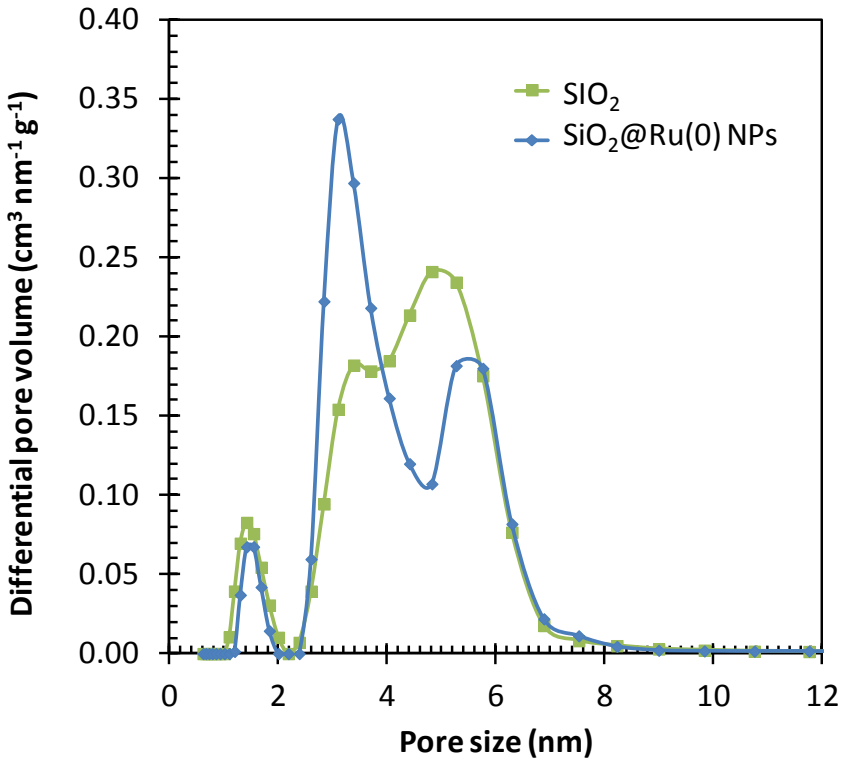

Figure 2. Differential pore volume of SiO_2 and SiO_2@Ru(0) NPs variation with the pore size obtained with the Non Linear Density Functional Theory.

3.2 Theoretical and mathematical background

Atrazine was used as a HO° radical tracer using a low initial concentration (< 300 ppb) compared to the initial ozone concentrations (1-2 ppm) to limit its influence (and those of its byproducts) on the ozone decomposition kinetics. This compound has been preferred to para-chlorobenzoic acid (pCBA), which is more often used in ozonation studies, due to the acidic pH set for the experiments. Indeed, pCBA has a pKa (3.99) higher than the pH of the study (≈ 2.9), whereas atrazine pKa is lower (1.6) [27].

In aqueous phase, atrazine can react with O_3 and HO° through bimolecular reactions [27]. The reaction rate can be written according to Eq. 1:

$$-\frac{dC_{at}}{dt} = k_1 C_{at} C_{HO^\circ} + k_2 C_{at} C_{O3} \qquad \text{Eq. 1}$$

C_{O3}, $C_{HO°}$ and C_{at} are respectively the ozone, hydroxyl radical and atrazine concentrations. k_1 (= 3×10^9 L mol^{-1} s^{-1}) and k_2 (=5.71 L mol^{-1} s^{-1} at pH = 2.9) are the second-order kinetic constants of the reaction of atrazine with respectively HO° and O_3 [27, 35].

Since ozone and atrazine concentrations are measured over time, their concentration can be modeled satisfactorily using n^{th} order rate equations:

$$-\frac{dC_j}{dt} = k_j C_j^{\,n_j} \qquad \text{Eq. 2}$$

The subscript j refers to O_3 or atrazine. k_j (mol^{1-n_j} L^{n_j-1} s^{-1}) and n_j (no unit) are respectively the apparent kinetic constants and the order of reaction associated to the species j consumption. They can be determined by numerical resolution for each experiment trying to minimize the least square error function based on the experimental and modeled concentrations. By integration between t_0 and t, the concentration of the species j evolution over time can be determined as a function of the initial concentration ($C_j^{t=0}$), k_j and n_j according to Eq. 4:

$$\int_{C_j^{t=0}}^{C_j^t} \frac{dC_j}{C_j^{\,n_j}} = -\int_{t_0}^{t} k_j dt \qquad \text{Eq. 3}$$

$$\Rightarrow C_j = \left(C_j^{t=0} + (n_j - 1)k_j t\right)^{n_j - 1} \qquad \text{Eq. 4}$$

The half-life time of the species j $\left(C_j = C_j^{t=0}/2\right)$ is then determined by Eq. 5:

$$t_{1/2} = \frac{\left(C_j^{t=0}\right)^{1-n_j}\left(2^{n_j-1}-1\right)}{(n_j-1)k_j} \qquad \text{Eq. 5}$$

For the particular case $n_j = 1$ (first-order), the following equation must be used instead of Eq. 4:

$$\Rightarrow C_j = C_j^{t=0}\exp(-k_j t) \qquad \text{Eq. 6}$$

The R_{ct} ratio is currently used to evaluate the HO° exposure to the O_3 exposure during a time interval ranging between t_i and t_{i+1} [36]:

$$R_{ct} = \frac{\int_{t_i}^{t_{i+1}} C_{HO^\circ} dt}{\int_{t_i}^{t_{i+1}} C_{O3} dt} \quad \text{Eq. 7}$$

The instantaneous R_{ct} ratio can be also calculated. Indeed, Eq. 1 can be integrated between t_i and t_{i+1}:

$$-\int_{C_{at}^{t_i}}^{C_{at}^{t_{i+1}}} \frac{dC_{at}}{C_{at}} = \int_{t_i}^{t_{i+1}} \left(k_1 C_{HO^\circ} + k_2 C_{O3}\right) dt \quad \text{Eq. 8}$$

According to Eqs 7 and 8:

$$\ln\left(\frac{C_{at}^{t_i}}{C_{at}^{t_{i+1}}}\right) = \left(k_1 R_{ct} + k_2\right) \int_{t_i}^{t_{i+1}} C_{O3} dt \quad \text{Eq. 9}$$

$$\Rightarrow R_{ct} = \frac{1}{k_1}\left[\frac{\ln\left(\frac{C_{at}^{t_i}}{C_{at}^{t_{i+1}}}\right)}{\int_{t_i}^{t_{i+1}} C_{O3} dt} - k_2\right] \quad \text{Eq. 10}$$

From Eq. 10, the parameter R_{ct} can be simply deduced over time using the ozone and atrazine concentrations deduced from the model (Eq. 4) instead of the experimental concentrations to limit error propagation. The ozone exposure is simply determined by discretization:

$$\int_{t_i}^{t_{i+1}} C_{O3} dt = \frac{\left(C_{O3}^{t=0} + \left(n_{O3} - 1\right) k_{O3} t_i\right)^{n_{O3}-1} + \left(C_{O3}^{t=0} + \left(n_{O3} - 1\right) k_{O3} t_{i+1}\right)^{n_{O3}-1}}{2} \left(t_{i+1} - t_i\right) \quad \text{Eq. 11}$$

The transient HO° concentration can be also calculated, which can be useful for the total HO° radical exposure evaluation. From Eq. 2:

$$-\frac{dC_{at}}{dt} = k_1 C_{at} C_{HO^\circ} + k_2 C_{at} C_{O3} \Rightarrow k_{at} {C_{at}}^{n_{at}} = k_1 C_{at} C_{HO^\circ} + k_2 C_{at} C_{O3} \quad \text{Eq. 12}$$

$$\Rightarrow C_{HO^\circ} = \frac{k_{at} {C_{at}}^{n_{at}-1} - k_2 C_{O3}}{k_1} \quad \text{Eq. 13}$$

Here, the atrazine and ozone concentrations refer to those from the model. Therefore Eq. 13 can be rewritten:

$$\Rightarrow C_{HO^\circ} = \frac{k_{at}\left(\left(C_{at}^{t=0} + \left(n_{at} - 1\right) k_{at} t_i\right)^{n_{at}-1}\right)^{n_{at}-1} - k_2 \left(C_{O3}^{t=0} + \left(n_{O3} - 1\right) k_{O3} t_i\right)^{n_{O3}-1}}{k_1} \quad \text{Eq. 14}$$

3.3 Reference experiments

Several reference experiments were performed at pH ≈ 2.9 to assess rigorously the influence of the catalysts on the ozone decomposition and radical production.

First, experiments without ozone showed a negligible adsorption of atrazine on each catalyst. Therefore, the atrazine consumption observed in the presence of ozone could only be attributed to oxidation reactions.

Secondly, experiments without catalyst were performed to assess the influence of atrazine on the ozone decomposition. No significant differences were observed concerning the ozone decomposition kinetics with or without atrazine. The ozone half-life time was in the range larger than 10^4 s. The R_{ct} evaluated using Eq. 10 was equal to 2.9×10^{-9}, thus revealing a low HO° concentration at acidic pH as expected.

Thirdly, the influence of atrazine in solution on the ozone decomposition kinetics was assessed in the presence of catalyst. In that case, even using very low atrazine concentrations, the ozone decomposition was a little bit enhanced with a half-life time reduced by 10-20%. This influence is low compared to intrinsic influence of the catalysts on the kinetics.

3.4 Evaluation of TiO_2 or SiO_2–supported ruthenium nanocatalysts

The supported-Ru(0) catalysts (SiO_2@Ru(0) NPs and TiO_2@Ru(0) NPs), with a low metal loading (0.1% wt.), have been evaluated for the ozone decomposition and HO° radical production and compared with the supports alone (SiO_2 and TiO_2). The influence of the concentration has been studied for each catalyst (250, 500 and 1000 mg L^{-1}). Fig. 3 shows an example of the ozone and atrazine concentration profiles obtained during an experiment. The straight lines correspond to the n^{th} order models developed for each species (Eq. 4).

Table 1 summarizes all the results gathered using increasing concentrations of the supported-ruthenium (0) nanocatalysts, and of the unloaded support. The agreement between the experimental ozone and atrazine concentrations and those deduced from the models (Eq. 4) is expressed for each experiment by the determination coefficient R^2. A good agreement is obtained for atrazine (whose analytical procedure is robust) but is usually more mitigated for ozone (whose analysis is known to be difficult and suffers from rather high uncertainties).

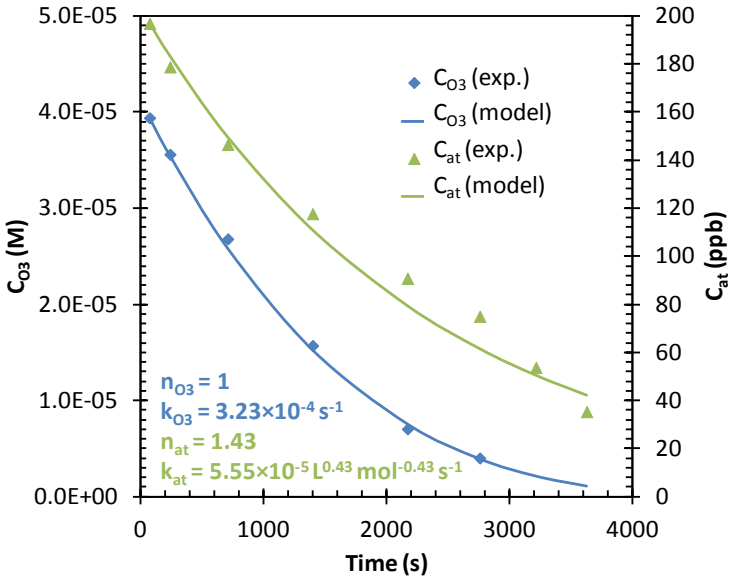

Figure 3. Example of ozone and atrazine concentration profiles (SiO_2 without NPs at 500 mg L^{-1}).

Table 1. Main results obtained using supported-Ru(0) NPs and supports alone. The determination coefficients (R^2) indicate the good correlation between the model (Eq. 4) and the experimental concentrations. The values of the 2 last columns are calculated from Eqs 15 and 16.

Catalyst	Mass of Ru impregnated (mg)	Concentration (mg L^{-1})	O_3 consum.		At. consumption		HO° prod.	
			$t_{1/2}$ (s)	R^2 (%)	$t_{1/2}$ (s)	R^2 (%)	∫[HO]dt	R_{ct}
No catalyst			> 10^4	87.00	4500	98.30	Not signif.	2.9×10^{-9}
SiO_2	No Ru impregnated	250	1841	87.00	4092	99.66	2.0×10^{-10}	2.8×10^{-9}
		500	2147	98.40	1373	99.76	6.2×10^{-10}	7.3×10^{-9}
		1000	3365	94.95	986	99.62	9.0×10^{-10}	5.9×10^{-9}
SiO_2@Ru(0) NPs	0.1% (m/m)	250	1005	99.75	1603	98.58	3.0×10^{-10}	6.5×10^{-9}
		500	333	94.61	619	99.64	3.7×10^{-10}	2.9×10^{-8}
		1000	272	99.61	436	97.99	4.5×10^{-10}	2.6×10^{-8}
TiO_2	No Ru impregnated	250	4101	91.17	3119	99.44	6.6×10^{-10}	3.8×10^{-9}
		500	4390	94.84	2032	99.63	5.4×10^{-10}	3.9×10^{-9}
		1000	1741	89.83	2712	99.04	4.1×10^{-10}	5.2×10^{-9}
TiO_2@Ru(0) NPs	0.1% (m/m)	250	579	88.62	1158	99.87	5.9×10^{-10}	2.0×10^{-8}
		500	258	89.28	699	99.39	4.0×10^{-10}	2.9×10^{-8}
		1000	238	87.42	525	99.67	3.0×10^{-10}	2.8×10^{-8}

Table 1 and Fig. 4 (a) emphasize a significant ozone decomposition enhancement, even using non-doped catalysts. Indeed, using the non-doped catalyst, the ozone half-life time decreases by a factor 2 to 3, compared to the reference experiment without any catalyst. On the one hand, the use of metal oxide such as TiO_2 as catalyst for ozonation is rather well documented [7, 8]. According to Kasprzyk-Hordern et al. (2003), both Brönsted (hydroxyl groups at the catalyst surface) and Lewis acid (located on the metal cation) sites are supposed to be the catalytic centers in TiO_2 catalysts. Nonetheless, the ozone decomposition enhancement using TiO_2 alone remains limited. This result is not surprising since the poorly active (in ozonation) anatase form was used and the specific area was low (around 50 $m^2\ g^{-1}$) [7]. On the other hand, SiO_2 is classically used in heterogeneous catalytic ozonation, only doped with metals [8]. Contrary to TiO_2, which is capable of both ion and ligand exchange, SiO_2 could only exchange cations. Nonetheless, SiO_2 alone enhances the ozone decomposition. Even if the potential of SiO_2 alone as catalyst for heterogeneous ozone is not documented in the literature, its influence on the ozone decomposition has been already demonstrated [37]. The initiation of the ozone decomposition by silica and glass is attributed to collision, adsorption and/or energy effects. Owing to the high silica surface area (around 450 $m^2\ g^{-1}$), the ozone decomposition observed in this study could be reasonably due to these effects. The ozone

decomposition enhancement surprisingly decreases with the concentration, which could traduce an antagonist role played by SiO_2 as an initiator and scavenger of the ozone decomposition [38].

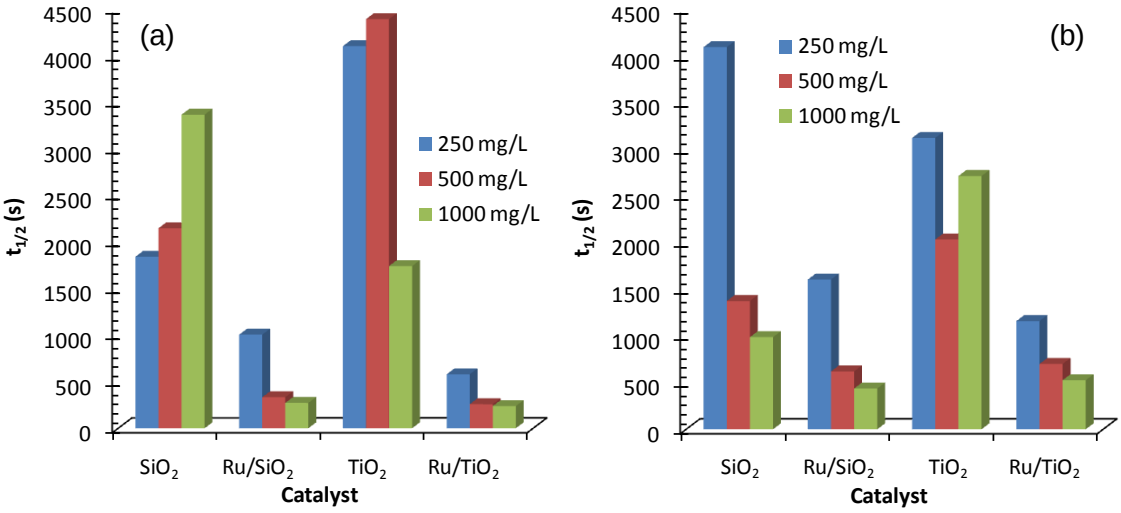

Figure 4. (a) Ozone and (b) atrazine half-life times observed for the 4 catalysts at different catalyst concentrations.

Using the supported-Ru(0) nanocatalysts, the reaction kinetics is greatly improved, since the ozone half-life time drops by a factor 20-30 compared to a non-catalyzed reaction. The results obtained for both supports are comparable even if the ozone decomposition strongly depends on the metal-support interactions [6]. The ozone half-life time decreases with the catalyst concentration, which can traduce a predominant initiator behavior. These results demonstrate that Ru(0) nanospecies have a beneficial effect in the ozonation process, enhancing the catalytic activity. Moreover, although XRD analyses could not confirm the presence of Ru nanospecies owing to the very low metal loading, these enhanced kinetics undoubtedly proved the presence of the ruthenium species on the inorganic support.

A first approach to evaluate the potential of these catalysts for micropollution removal relies on the comparison of the atrazine half-life times for the various catalysts at different concentrations (Fig. 4 (b) and table 1). Except for TiO_2 which presents no consistent trend, the atrazine half-life time decreases when increasing the amount of catalyst. This is noteworthy with the ruthenium doped catalysts, showing the great effect of the Ru NPs in the catalytic ozonation reaction. Indeed, in the

absence of catalyst, the atrazine half-life time is around 4500 s. As a consequence, the synthesized catalysts enable to enhance at the same time the ozone and atrazine consumption, which is justified by a higher transient radical concentrations (in the liquid phase and/or at the gas-liquid interface) during a short reaction time. Nevertheless, this enhancement must not be counterbalanced by a decrease in the total hydroxyl radical production for a given initial ozone concentration, which would imply a higher oxidant dosage to compensate.

A second approach to validate the use of these catalysts for micropollutant removal consists in calculating the hydroxyl radical production. Even if there is no experimental confirmation that atrazine is oxidized in solution or at the gas-liquid interface by ozone and free hydroxyl radicals, the determination of the HO° concentration and of the R_{ct}, following the numerical procedure developed earlier (section 3.2), could enable to evaluate the catalyst activity as an equivalent of free radicals and to compare the catalytic ozonation to other usual ozonation processes, involving only free hydroxyl radicals and ozone as active species (peroxone, homogeneous catalytic ozonation, etc.). The HO° radical exposure can be calculated through Eq. 15 with C_{HO° calculated from Eq. 14:

$$\int_{t_0}^{t} C_{HO^\circ} dt = \sum_{i=0}^{n-1} \frac{C_{HO^\circ}^{t_i} + C_{HO^\circ}^{t_{i+1}}}{2} \left(t_{i+1} - t_i\right) \qquad \text{Eq. 15}$$

The last raw of Table 1 summarizes the hydroxyl radical exposure obtained from Eq. 15 for the different catalysts at 90% of the initial ozone concentration consumption. This exposure is divided by the corresponding ozone exposure to get the R_{ct} ratio [36]:

$$R_{ct} = \int_{t_0}^{t} C_{HO^\circ} dt \Big/ \int_{t_0}^{t} C_{O3} dt \qquad \text{Eq. 16}$$

The last raw of Table 1 and Fig. 5.a undoubtedly emphasizes that the use of the Ru(0) doped catalysts improves the radical production since 2 to 3 more HO° are produced, compared to undoped catalysts, confirming the potential of these catalysts for micropollutant removal. The R_{ct} ratio indicated in Table 1 and Fig. 5 represents the average R_{ct} ratio determined between t_0 and the time necessary to decompose 90% of the initial ozone concentration. The instantaneous R_{ct} ratio

calculated from Eq. 10 increases over time (Fig. 5.b). This positive behavior is balanced by a decreasing of the ozone exposure which leads to a HO° concentration decreasing, but slower than expected.

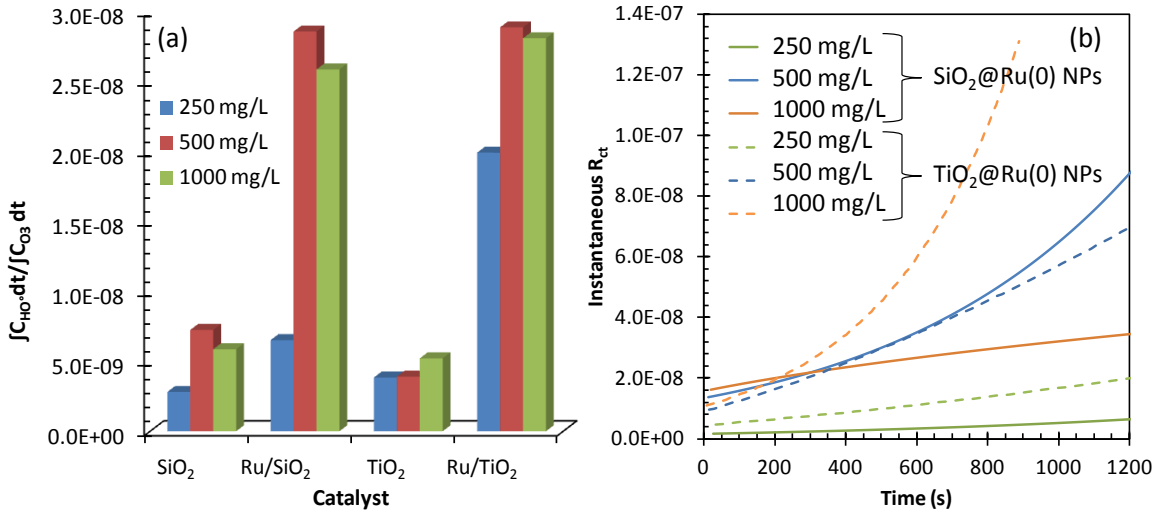

Figure 5. (a) R_{ct} (from Eq. 16) at 90% of the initial ozone consumption observed for the 4 catalysts at various catalyst concentrations. (b) Instantaneous R_{ct} evolution for the Ru-supported catalysts at various catalyst concentrations.

3.5 Investigation of a non-woven fiber paper as support for ruthenium nanoparticles in ozonation processes

The Ru(0) NPs deposited on inorganic powder support (SiO_2 or TiO_2) demonstrated a good potential for ozone decomposition enhancement and HO° radical production. However, these catalysts must be recovered and recycled by filtration from the purified solution. This step could be avoided by using metal NPs directly supported on a fixed support such as a non-woven fiber paper coated with a mixture of TiO_2, SiO_2 and zeolite as investigated in this article. This original support was impregnated with two different Ru loadings, using a percolation approach:

- a similar loading as for the TiO_2 or SiO_2@Ru(0) NPs (0.1% wt.) at 500 mg L^{-1}, corresponding to 1 mL of colloidal suspension, *i.e.* approximately 0.5 mg of Ru (see material and methods section) ;
- a saturated material, which corresponds to 7 mL of an aqueous suspension of Ru(0) NPs.

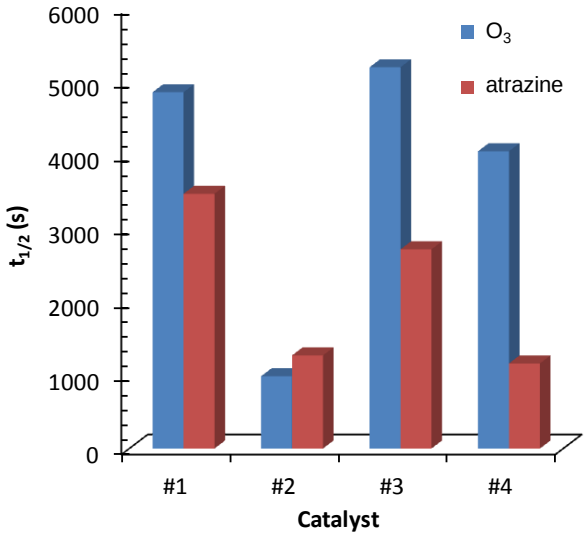

Figure 6. Ozone and atrazine half-life times observed for the 4 paper catalysts.

The influence of the drying temperature during the catalyst's preparation, either ambient temperature (20°C) or 60°C using a thermostatic chamber, was studied on the catalytic ozonation results. The paper mass was identical for each experiment with a paper surface implemented of a few cm^2. The ozone and atrazine half-life times obtained during the batch experiments are

summarized in Table 2 and represented Fig. 6. First, concerning the effect of the drying temperature, better performances, both for ozone decomposition and atrazine consumption, were achieved using the paper dried in the thermostatic chamber (at 60°C). These results could be attributed to a better adsorption of the Ru(0) colloids at the material surface when the catalyst was dried at a higher temperature. Moreover, the ruthenium loading of the nanocatalyst (0.1% wt. *vs*. saturated material) has also an influence on the catalytic activity. Indeed, best ozone decomposition kinetics was obtained using low Ru loaded material (Entries 1 and 2). Finally, at similar ruthenium loading (0.1% wt.) the ozone decomposition and atrazine consumption kinetics are significantly lower for the Ru(0) NPs deposited on the non-woven fiber paper (Table 2, Entry 2), compared to those supported on SiO_2 or TiO_2 (Table 1). These results could be attributed to internal and/or external diffusion limitations and in that case, they could be compensated by a higher mixing energy. Further investigations are ongoing to improve the catalytic activities of the Ru nanospecies deposited on the non-woven fiber paper.

Table 2. Main results obtained using paper-supported Ru(0) catalysts. The determination coefficients (R^2) indicate the agreement between the model (Eq. 4) and the experimental concentrations. The values of the 2 last columns are calculated from Eqs 15 and 16.

Exp. N°	Ru mass (mg)	Drying T (°C)	O_3 consum.		At. consumption		HO° prod.	
			$t_{1/2}$ (s)	R^2 (%)	$t_{1/2}$ (s)	R^2 (%)	∫[HO]dt	R_{ct}
#1	0.47	20	4850	99.00	3468	95.95	1.41×10^{-10}	1.96×10^{-9}
#2	0.47	60	984	97.60	1267	98.45	1.70×10^{-10}	1.38×10^{-8}
#3	3.3	20	5190	89.83	2712	99.04	5.33×10^{-10}	6.76×10^{-9}
#4	3.3	60	4047	88.62	1158	99.87	7.44×10^{-10}	2.36×10^{-8}

Finally, the amount of radical species produced either by powder or paper catalysts, estimated through Eq. 16, are comparable (Tables 1 and 2). Consequently, both catalysts present the same potential for radical production but in a shorter time for powder supports, which traduces a better catalytic activity for ozone decomposition.

4. Conclusion and perspectives

To conclude, Ru(0) NPs, deposited on powder supports (SiO_2 or TiO_2), have been studied as catalysts for ozone decomposition and radical production in batch experiments using atrazine at low concentrations as a radical tracer. Significant enhancements of the ozone decomposition and atrazine consumption kinetics have been measured using the ruthenium-doped supports, compared to the supports alone, thus showing the beneficial role of the Ru(0) nanospecies in the radical production. Further investigations are ongoing to determine the influence of the pH, the mass-transfer limitations and the NPs concentration. Moreover, this potential should be confirmed using pollutants at realistic industrial concentrations in natural water. Besides, since the catalyst stability in combination with strong oxidants such as ozone is of major concern for future applications, the durability of the developed catalysts will be assessed in the future. Up to now, no Ru leaching has been observed during a 24h continuous ozonation in a gas-liquid contactor fed with O_3 at 100 mg Nm^{-3}.

The comprehension of the chemical mechanism is still under questioning. The confirmation of free hydroxyl radical production will be assessed using tertiobutanol as radical scavenger to appreciate the ozone decomposition inhibition and/or by using teraphtalic acid whose reaction product with HO° is fluorescent. These experiments are planned on continuous and semi-continuous gas-liquid reactors instead of the homogeneous reactor presented in this paper, which was particularly helpful for the primary catalyst comparison but far away from realistic treatment conditions.

The use of a non-woven fiber paper coated with a mixture of TiO_2, SiO_2 and zeolite has been investigated as an original and innovative support for metallic nanospecies. Although lower kinetics was observed for ozone decomposition, the developed catalyst could be promising for industrial applications and further investigations are ongoing to improve the catalytic activity. The ability of this material to survive over a long period will be assessed in the future.

Funding source

The results that are presented in this article have been granted by the French Higher Education and Research Ministry (MESR) and the Institute of Chemical Sciences of Rennes (UMR CNRS 6226).

Acknowledgements

We are very grateful to Sylvain GIRAUDET (ENSCR) for its assistance with the Quantachrome instruments, to Eric LE FUR (ENSCR) for the XRD analysis and Patricia BEAUNIER (UPMC) for TEM experiments.

References

[1] U. Von Gunten, Ozonation of drinking water: Part I. Oxidation kinetics and product formation, Water Research 37 (2003) 1443-1467.

[2] M. Deborde, U. Von Gunten, Reactions of chlorine with inorganic and organic compounds during water treatment - Kinetics and mechanisms: A critical review, Water Research 42 (2008) 13-51.

[3] R. Andreozzi, V. Caprio, A. Insola, R. Marotta, Advanced oxidation processes (AOP) for water purification and recovery, Catalysis Today 53 (1999) 51-59.

[4] R. Munter, Advanced Oxidation Processes – Current status and prospects, Proceedings of the Estonian Academy of Sciences 50 (2001) 59-80.

[5] F.J. Beltrán, Ozone reaction kinetics for water and wastewater systems, CRC Press, Boca Raton, 2004.

[6] J. Staehelin, J. Hoigne, Decomposition of ozone in water: rate of initiation by hydroxide ions and hydrogen peroxide, Environmental Science & Technology 16 (1982) 676-681.

[7] J. Nawrocki, B. Kasprzyk-Hordern, The efficiency and mechanisms of catalytic ozonation, Applied Catalysis B: Environmental 99 (2010) 27-42.

[8] B. Kasprzyk-Hordern, M. Ziółek, J. Nawrocki, Catalytic ozonation and methods of enhancing molecular ozone reactions in water treatment, Applied Catalysis B: Environmental 46 (2003) 639-669.

[9] H. Zhao, Y. Dong, P. Jiang, G. Wang, J. Zhang, C. Zhang, $ZnAl_2O_4$ as a novel high-surface-area ozonation catalyst: One-step green synthesis, catalytic performance and mechanism, Chemical Engineering Journal 260 (2015) 623-630.

[10] H. Jung, H. Choi, Catalytic decomposition of ozone and para-Chlorobenzoic acid (pCBA) in the presence of nanosized ZnO, Applied Catalysis B: Environmental 66 (2006) 288-294.

[11] N. Pugazhenthiran, P. Sathishkumar, S. Murugesan, S. Anandan, Effective degradation of acid orange 10 by catalytic ozonation in the presence of Au-Bi_2O_3 nanoparticles, Chemical Engineering Journal 168 (2011) 1227-1233.

[12] H. Jung, H. Park, J. Kim, J.-H. Lee, H.-G. Hur, N.V. Myung, H. Choi, Preparation of Biotic and Abiotic Iron Oxide Nanoparticles (IOnPs) and Their Properties and Applications in Heterogeneous Catalytic Oxidation, Environmental Science & Technology 41 (2007) 4741-4747.

[13] Y. Yang, J. Ma, Q. Qin, X. Zhai, Degradation of nitrobenzene by nano-TiO_2 catalyzed ozonation, Journal of Molecular Catalysis A: Chemical 267 (2007) 41-48.

[14] H. Jung, J. Kim, H. Choi, J. Lee, H. Hur, Synthesis of nanosized biogenic magnetite and comparison of its catalytic activity in ozonation, Applied Catalysis B: Environmental 83 (2008) 208-213.

[15] Y. Dong, G. Wang, P. Jiang, A. Zhang, L. Yue, X. Zhang, Catalytic Ozonation of Phenol in Aqueous Solution by Co_3O_4 Nanoparticles, Bulletin of the Korean Chemical Society 31 (2010) 2830-2834.

[16] Y. Dong, H. Yang, K. He, S. Song, A. Zhang, β-MnO_2 nanowires: A novel ozonation catalyst for water treatment, Applied Catalysis B: Environmental 85 (2009) 155-161.

[17] H. Zhao, Y. Dong, G. Wang, P. Jiang, J. Zhang, L. Wu, K. Li, Novel magnetically separable nanomaterials for heterogeneous catalytic ozonation of phenol pollutant: $NiFe_2O_4$ and their performances, Chemical Engineering Journal 219 (2013) 295-302.

[18] H. Zhao, Y. Dong, P. Jiang, G. Wang, J. Zhang, K. Li, An insight into the kinetics and interface sensitivity for catalytic ozonation: the case of nano-sized $NiFe_2O_4$, Catalysis Science & Technology 4 (2014) 494-501.

[19] Z.Q. Liu, B.J. Han, J. Ma, R.G. Zha, H.T. Zhu, L.P. Shen, W.P. Guan, S.J. Wang, L. Zhao, Catalytic ozonation and its full scale application in China in the last decade (2000-2010), IOA IUVA World Congress and ExhibitionParis, France, 2011.

[20] L. Zhao, J. Ma, Z.-z. Sun, X.-d. Zhai, Catalytic ozonation for the degradation of nitrobenzene in aqueous solution by ceramic honeycomb-supported manganese, Applied Catalysis B: Environmental 83 (2008) 256-264.

[21] L. Zhao, Z. Sun, J. Ma, Novel relationship between hydroxyl radical initiation and surface group of ceramic honeycomb supported metals for the catalytic ozonation of nitrobenzene in aqueous solution, Environmental Science & Technology 43 (2009) 4157-4163.

[22] L. Zhao, J. Ma, Z. Sun, H. Liu, Mechanism of heterogeneous catalytic ozonation of nitrobenzene in aqueous solution with modified ceramic honeycomb, Applied Catalysis B: Environmental 89 (2009) 326-334.

[23] P. Sonström, B. Halbach, S.T. Djakpou, B. Ritz, K. Ahrenstorf, G. Grathwohl, H. Weller, M. Bäumer, Foam, fleece and honeycomb: catalytically active coatings from colloidally prepared nanoparticles, Catalysis Science & Technology 1 (2011) 830-838.

[24] N.K.V. Leitner, F. Delanoë, B. Acedo, B. Legube, Reactivity of various Ru/CeO_2 catalysts during ozonation of succinic acid aqueous solutions, New Journal of Chemistry 24 (2000) 229-233.

[25] C. Hubert, E. Guyonnet-Bilé, A. Denicourt-Nowicki, A. Roucoux, Rh(0) colloids supported on TiO_2: a highly active and pertinent tandem in neat water for the hydrogenation of aromatics, Green Chemistry 13 (2011) 1766-1771.

[26] L. Barthe, A. Denicourt-Nowicki, A. Roucoux, K. Philippot, B. Chaudret, M. Hemati, Model arenes hydrogenation with silica-supported rhodium nanoparticles: The role of the silica grains and of the solvent on catalytic activities, Catalysis Communications 10 (2009) 1235-1239.

[27] F.J. Beltrán, J.F. Garcia-Araya, B. Acedo, Advanced oxidation of atrazine in water. I: Ozonation, Water Research 28 (1994) 2153-2164.

[28] C.L. Bianchi, C. Pirola, V. Ragaini, E. Selli, Mechanism and efficiency of atrazine degradation under combined oxidation processes, Applied Catalysis B: Environmental 64 (2006) 131-138.

[29] C. Hubert, E.G. Bilé, A. Denicourt-Nowicki, A. Roucoux, Tandem dehalogenation–hydrogenation reaction of halogenoarenes as model substrates of endocrine disruptors in water: Rhodium nanoparticles in suspension vs. on silica support, Applied Catalysis A: General 394 (2011) 215-219.

[30] A. Nowicki, V. Le Boulaire, A. Roucoux, Nanoheterogeneous Catalytic Hydrogenation of Arenes: Evaluation of the Surfactant-Stabilized Aqueous Ruthenium(0) Colloidal Suspension, Advanced Synthesis & Catalysis 349 (2007) 2326-2330.

[31] E. Guyonnet-Bilé, R. Sassine, A. Denicourt-Nowicki, F. Launay, A. Roucoux, New ammonium surfactant-stabilized rhodium(0) colloidal suspensions: Influence of novel counter-anions on physico-chemical and catalytic properties, Dalton Transactions 40 (2011) 6524-6531.

[32] A. Denicourt-Nowicki, A. Roucoux, From hydroxycetylammonium salts to their chiral counterparts. A library of efficient stabilizers of Rh(0) nanoparticles for catalytic hydrogenation in water, Catalysis Today 247 (2015) 90-95.

[33] J. Hoigne, Inter-calibration of OH radical sources and water quality parameters, Water Science and Technology 35 (1997) 1-8.

[34] J. Landers, G.Y. Gor, A.V. Neimark, Density functional theory methods for characterization of porous materials, Colloids and Surfaces A: Physicochemical and Engineering Aspects 437 (2013) 3-32.

[35] J.L. Acero, K. Stemmler, U. Von Gunten, Degradation kinetics of atrazine and its degradation products with ozone and OH radicals : a predictive tool for drinking water treatment, Environmental Science & Technology 34 (2000) 591-597.

[36] M.S. Elovitz, U. Von Gunten, Hydroxyl radical/ozone ratios during ozonation processes. I. The R_{ct} concept, Ozone Science and Engineering 21 (1999) 239-260.

[37] A. Ouederni, Q. Limvorapituk, R. Bes, J.C. Mora, Ozone decomposition on glass and silica, Ozone: Science & Engineering 18 (1996) 385-416.

[38] E.L. Yong, Y.-P. Lin, Incorporation of initiation, promotion and inhibition in the R_{ct} concept and its application in determining the initiation and inhibition capacities of natural water in ozonation, Water Research 46 (2012) 1990-1998.